PROCEEDINGS OF THE ROYAL SOCIETY A

Proc. R. Soc. A (2005) **461**, 3871–3892
doi:10.1098/rspa.2005.1514
Published online 30 September 2005

Wave propagation in shape memory alloy rods under impulsive loads

By Yi-Chao Chen[1] and Dimitris C. Lagoudas[2]

[1]*Department of Mechanical Engineering, University of Houston, Houston, TX 77204, USA*
(chen@uh.edu)
[2]*Aerospace Engineering Department, Texas A&M University, College Station, TX 77843, USA*
(lagoudas@aeromail.tamu.edu)

A dynamic analysis is given of the wave propagation in a polycrystalline shape memory alloy semi-infinite rod subject to an impulsive load described by a rectangular loading function. This is a continuation of the previous study for which the impact load is described by a step loading function, and for which the rod undergoes martensitic phase transformation only. In the presence of unloading, the rod also undergoes reverse transformation from martensite to austenite. A maximum internal dissipation criterion is proposed to select a unique dynamic solution, in which an elastic unloading wave front precedes the reverse transformation wave front. This elastic unloading wave will meet with the forward transformation wave at a later time, leading to a sequence of wave encounters and progressively more complicated profiles of the state variables. The asymptotic behaviour of the solution and the energy dissipation are discussed.

Keywords: dynamics; phase transformation; shock waves; dissipation; polycrystalline material

1. Introduction

In a previous paper, Chen & Lagoudas (2000) studied the dynamic solution of a shape memory alloy (SMA) semi-infinite rod subject to an impact load defined by a step loading function. One of the focuses of the work is on the initiation and propagation of stress waves and phase transformation fronts in the rod. The material behaviour of the shape memory alloy is modelled by a thermomechanical constitutive theory developed by Lagoudas *et al.* (1996) for polycrystalline Ni–Ti alloys. A typical solution involves two wave fronts which are initiated at the impact surface and propagate into the rod. One, travelling at the acoustic speed, separates the tranquil and disturbed regions. The other, travelling at a lower speed, separates the regions of the martensitic and austenitic phases. Because the stress of the step loading function remains constant after the impact, the wave pattern is unaltered with the two wave fronts propagating indefinitely without interference with each other.

Received 5 February 2004
Accepted 10 May 2005

A similar problem was studied by Bekker *et al.* (2002) for various constitutive functions. Both isothermal and adiabatic analyses are presented. In this work, the jump conditions are not explicitly introduced and the numerical solutions of the field equations are obtained by using a Lax–Friedrichs finite-difference scheme. Nevertheless, the numerical solutions do show narrow regions where the values of the state variables change rapidly. This is consistent with the practice of allowing non-smooth solutions which satisfy the jump conditions.

A combined numerical and experimental investigation of the dynamic loading of polycrystalline SMA rods was recently given by Lagoudas *et al.* (2003). The numerical simulations utilise a finite-element method. The energy dissipation is evaluated for a square pulse stress input. The dynamic response of a NiTi SMA rod is also studied experimentally in a split Hopkinson bar apparatus under detwinning conditions. Strain history records obtained by strain gauges placed at different locations along the SMA rod are compared with numerical simulations.

In many practical problems, an impact load is impulsive with a short time duration. A rectangular loading function is often used to model such an impact load. Under this loading function, the dynamic solution during loading is identical to that for the step loading function. Once unloading takes place, however, the solution becomes drastically more complicated. Not only will two new wave fronts emerge at unloading, the wave pattern will no longer be unaltered afterwards. An infinite sequence of wave encounters will occur, giving rise to a rapidly increasing number of moving regions of different states. As a result of wave encounters, energy dissipates, and the rod will eventually reach a state in which only a fraction of the input energy is being carried forward. The purpose of this paper is to study such a dynamic solution.

The mathematical theory of dynamics of continuous media is fairly well developed. Expositions of the basic theory can be found, for example, in Courant & Friedrichs (1956), Bland (1969) and Lax (1973). More contemporary treatments of the topic, that involve material phase transformations in solids, can be found in James (1980), Pence (1986, 1991, 1992) and Abeyaratne & Knowles (1991, 1994*a*,*b*). In these works, the constitutive functions of nonlinear elasticity are used. Moving or stationary phase boundaries are associated with multi-well potential energy functions. Also included in Abeyaratne & Knowles' theory are a kinetic relation and a nucleation criterion for the motion of phase boundaries. Such a theory appears to be particularly suitable to model SMA single crystals.

In the present work, we use the constitutive theory developed by Lagoudas *et al.* (1996) for SMA polycrystals. Besides the austenitic phase and the martensitic phase, there is a continuous spectrum of partial phases characterized by a parameter, the martensitic volume fraction. The constitutive theory also contains an internal variable, the transformation strain, which is determined by a transformation equation in relation to the martensitic volume fraction. Another feature of the present work is the choice of the rectangular loading function with prescribed time duration and stress level. While this loading function is suitable for modelling impulsive loads in real physical situations, we have been unable to find the corresponding dynamic analysis for solids that can undergo phase transformations. In addition, full consideration is given to the thermal effect, coupled with the mechanical effect and the material phase transformation. In particular, temperature and the balance of energy are analysed in this work.

In §2, we formulate the dynamic problem to be studied. The field equations and jump equations for various balance laws are introduced. The assumption of adiabatic processes is rationalized, and the constitutive theory for the polycrystalline SMA is described.

The structure of dynamic solutions for materials with piecewise linear stress–strain relation under piecewise constant initial and boundary conditions is discussed in §3. The solutions have a distinct simplicity of being piecewise constant. These solutions can be found by solving the jump equations, which are algebraic equations. It should be noted that even when the stress–strain relation is not piecewise linear, a piecewise constant solution determined by the jump equations still satisfies the balance laws precisely, as do many other solutions, smooth or non-smooth.

This issue of non-uniqueness is addressed in §4. Inspired by the work of Dafermos (1973), we require that the admissible solution must have maximum internal dissipation, which is defined as the difference between the rate of change of entropy per unit coldness (reciprocal of temperature) and the power of thermodynamic force associated with the phase transformation. A graphic representation of this maximum dissipation criterion is presented, which is used subsequently for selecting a unique piecewise constant solution.

In §5, the constitutive function proposed by Lagoudas *et al.* (1996) is used in the dynamic analysis. It is found that the stress–strain relation in a complete loading–unloading cycle is approximately piecewise linear. Hence, the piecewise constant solution selected by the maximum dissipation criterion is close to the exact solution, which may not be piecewise constant in general.

The dynamic solution during loading is studied in §6. The piecewise constant solution contains two shock waves: an elastic loading wave and a phase transformation wave. Divided by these waves are three regions of constant state variables: the tranquil region, the region at the start of martensitic transformation, and the region of the full martensitic phase. Such a solution is essentially identical to that in the previous work (Chen & Lagoudas 2000).

Section 7 concerns the dynamic solution at the initial stage of unloading. The solution has a similar characteristic to that at loading. Two additional wave fronts are initiated upon unloading. One corresponds to elastic unloading, and the other to reverse phase transformation. Hence, there are altogether four wave fronts propagating in the rod. As these waves pass a material point, it undergoes successively elastic loading to the martensitic start, then loading to full matensite at the impact stress, then elastic unloading to austenitic start, and finally to full austenite at zero stress. This sequence, however, will be interrupted once the elastic unloading wave meets with the forward martensitic transformation wave.

Such a wave encounter and the subsequent solution are studied in the concluding §8. It is found that a wave encounter generates at least three new waves. There are one or two progressing waves, one standing wave, and one or two reflecting waves. These waves and the state variables in various regions are determined by using the jump equations, the transformation equations, and the maximum dissipation criterion. More wave encounters take place at increasing frequency and density as time progresses. The asymptotic behaviour and the energy dissipation of the solution are discussed.

2. Basic formulae

We consider a semi-infinite rod, which will be modelled as a one-dimensional body. The rod is assumed to occupy the positive real axis $\mathbb{R}^+$, which is taken as the reference configuration, in the initial state. A material particle is represented by its coordinate $x \in \mathbb{R}^+$ in the reference configuration. We denote by $u(x,t)$ and $T(x,t)$, respectively, the displacement and the absolute temperature of the material point x at time t. The displacement u is assumed to be continuous and piecewise C^2 in the domain $\Omega \equiv \mathbb{R}^+ \times \mathbb{R}^+$ of space and time, and the temperature T is assumed[1] to be piecewise C^2 in Ω.

The strain ϵ and the velocity v are given by

$$\epsilon(x,t) = u_x(x,t), \quad v(x,t) = u_t(x,t), \tag{2.1}$$

where the subscripts x and t denote the partial derivatives with respect to these variables. The strain and the velocity must satisfy the compatibility condition

$$\epsilon_t = v_x \tag{2.2}$$

at a point where u is C^2.

In this work, we shall neglect body forces, external body heating source and heat conduction. The local form of the balance of linear momentum gives the following equation of motion

$$\rho v_t = \sigma_x, \tag{2.3}$$

where ρ is the constant mass density, and $\sigma(x,t)$ the stress field which is assumed to be piecewise C^1 in Ω. The value of σ is a measure of the resultant axial force over the cross-section of the rod. The local form of the balance of energy states

$$\rho\left(e + \frac{1}{2}v^2\right)_t = (\sigma v)_x, \tag{2.4}$$

where $e(x,t)$ is the internal energy. Here, the contribution of heat conduction to the energy balance has been omitted. The local form of the Clausius–Duhem inequality, as required by the second law of thermodynamics, states

$$\eta_t \geq 0, \tag{2.5}$$

where $\eta(x,t)$ is entropy.

A dynamic solution may be associated with moving surfaces, called shocks, across which various field quantities suffer jump discontinuities. The location of a shock can be identified by the material coordinate $s(t)$ of the particle which the shock is crossing at time t. The function s is assumed to be C^1. The jump of a function $f(x,t)$ at a shock $x = s(t)$ is defined by

$$[\![f]\!] = \lim_{\delta \to 0} [f(s(t) + \delta, t) - f(s(t) - \delta, t)]. \tag{2.6}$$

[1] In the presence of heat conduction, the temperature is expected to be continuous. The effect of heat conduction on the solution, however, is small compared to that of stress power and inertia for typical impact problems. This gives rise to solutions in which the temperature changes rapidly in some narrow regions known as shocks. An idealization of such solutions is made in the adiabatic analysis, as shall be assumed in this work, by neglecting heat conduction and allowing the temperature to be discontinuous across the shocks, which take the form of moving surfaces.

The kinematic compatibility, the balance of linear momentum, the balance of energy, and the Clausius–Duhem inequality at a shock lead to the following jump conditions:

$$s_t[\![\epsilon]\!] + [\![v]\!] = 0, \tag{2.7}$$

$$\rho s_t[\![v]\!] + [\![\sigma]\!] = 0, \tag{2.8}$$

$$\rho s_t[\![e + \frac{1}{2}v^2]\!] + [\![\sigma v]\!] = 0, \tag{2.9}$$

$$-s_t[\![\eta]\!] \geq 0. \tag{2.10}$$

The field equations (2.2)–(2.4) and the jump equations (2.7)–(2.9) are to be solved with the aid of constitutive equations. The rod is assumed to be composed of a shape memory alloy which is capable of undergoing stress- and thermal-induced phase transformations. In this work, we shall employ a one-dimensional version of the thermomechanical constitutive theory developed by Lagoudas *et al.* (1996). The derivation of the one-dimensional constitutive functions, based on the plane stress assumption, from the original three-dimensional theory is routine and omitted here for brevity.

The constitutive theory is formulated with Gibbs free energy G of the following form:

$$G = G(\sigma, T, \xi), \tag{2.11}$$

where ξ is martensitic volume fraction, which is a function of x and t, and takes values in [0,1]. The function $\xi(x,t)$ is assumed to be piecewise C^1 and may suffer jump discontinuity across a shock that separates two material phases. It must be noted that the constitutive function of the SMA is actually history dependent. The function relation in (2.11) displays only the state variable at the present time. Omitted are such parameters as the sign of ξ_t, and the values of ξ and G at the past time when ξ_t changed sign.

The strain consists of two parts

$$\epsilon = \epsilon^{\mathrm{e}} + \epsilon^{\mathrm{t}}, \tag{2.12}$$

where ϵ^{e} is the elastic strain, and ϵ^{t} the transformation strain. The Gibbs free energy is related to the internal energy through the following equation:

$$e = G + T\eta + \frac{1}{\rho}\sigma\epsilon^{\mathrm{e}}. \tag{2.13}$$

It follows from a standard argument in thermodynamics that the elastic strain ϵ^{e} and the entropy η are given by

$$\epsilon^{\mathrm{e}} = -\rho\frac{\partial G}{\partial \sigma}, \tag{2.14}$$

$$\eta = -\frac{\partial G}{\partial T}. \tag{2.15}$$

In the three-dimensional constitutive model of Lagoudas *et al.* (1996), no reorientation of martensitic variants is considered. For proportional loading, of

which the plane stress is a special case, the equation for the evolution of the transformation strain tensor and the evolution of the martensitic volume fraction can be integrated. The axial component of the resulting equation gives

$$\epsilon^{\mathrm{t}} = H\,\mathrm{sgn}(\sigma)\xi, \tag{2.16}$$

where H is a positive material constant corresponding to the maximum transformation strain.

The constitutive equation for the martensitic volume fraction ξ is derived from a dissipation potential theory. The thermodynamic force π conjugate to ξ is defined by

$$\pi = H|\sigma| - \rho\frac{\partial G}{\partial \xi}. \tag{2.17}$$

The phase transformation takes place when $|\pi|$ reaches a certain threshold value Y, which is a measure of the dissipation during the phase transformation. In the course of a forward martensitic phase transformation, the value of π equals Y, while ξ increases until it reaches 1. On the other hand, in a reverse phase transformation, π equals $-Y$, while ξ decreases until it reaches 0. Such processes can be described by the Kuhn–Tucker conditions

$$\pi\xi_t \geq 0, \quad (\pi^2 - Y^2)\xi_t = 0, \quad \pi^2 - Y^2 \leq 0 \qquad \text{if } 0 < \xi < 1. \tag{2.18}$$

The equations of energy balance (2.4) and (2.9) can be written in alternative forms. Substituting (2.13) into (2.4) and using (2.2), (2.3), (2.12) and (2.14)–(2.18), we find that

$$\rho\left(e + \frac{1}{2}v^2\right)_t - (\sigma v)_x = \rho T\eta_t - \pi\xi_t = \rho T\eta_t - Y|\xi_t| = 0. \tag{2.19}$$

It is observed that a solution of the last equation satisfies the entropy inequality (2.5). Also, it follows from (2.7)–(2.9), (2.12), (2.13) and (2.16) that

$$\rho s_t[\![e + \frac{1}{2}v^2]\!] + [\![\sigma v]\!] = s_t(\rho[\![G + T\eta]\!] + \langle\epsilon\rangle[\![\sigma]\!] - H[\![|\sigma|\xi]\!]) = 0, \tag{2.20}$$

where $\langle\cdot\rangle$ denotes the average of a function across the shock, e.g.

$$\langle\epsilon\rangle \equiv \lim_{\delta\to 0}\frac{1}{2}[\epsilon(s(t) + \delta, t) + \epsilon(s(t) - \delta, t)]. \tag{2.21}$$

3. Stress–strain curve. Piecewise constant solutions

Smooth solutions and jump solutions, satisfying (2.19) and (2.20), respectively, follow different stress–strain relations in general, due to the presence of dissipation associated with a jump solution. For either solution, the strain ϵ is related to the stress σ, the temperature T and the martensitic volume fraction ξ through equations (2.12), (2.14) and (2.16). Equations (2.17) and (2.18) can be used to determine ξ in terms of σ and T, and the energy balance equation, either (2.19) or (2.20), further determines T in terms of σ, thus leading to the stress–strain relation.

For typical Ni–Ti shape memory alloys, the stress–strain relation for smooth solutions, as determined by (2.12), (2.14) and (2.16)–(2.19), is approximately piecewise linear. That is, it is approximately linear in the austenitic phase, in the

martensitic phase, and during the phase transformations (forward or reverse). As a result, a solution can be approximated by one that corresponds to an appropriate piecewise linear stress–strain relation.

When the stress–strain relation is piecewise linear, the solutions of the dynamic problem enjoy a distinct simplicity, as has been exploited to a great extent in the work of Abeyaratne & Knowles (1991). Indeed, in this case, equation (2.2) becomes

$$S\sigma_t = v_x, \tag{3.1}$$

where S is the local constant elastic compliance. Equations (2.3) and (3.1) form a hyperbolic system of first order partial differential equations with constant coefficients. The general solution of this system is the well-known d'Alembert solution

$$\sigma = f(x + at) + g(x - at), \qquad v = Sa[f(x + at) - g(x - at)] + C, \tag{3.2}$$

where f and g are arbitrary functions, C an arbitrary constant, and a is the local acoustic speed given by

$$a \equiv \frac{1}{\sqrt{\rho S}}. \tag{3.3}$$

When initial and boundary conditions are given, the general solution (3.2) readily leads to the particular solution of the dynamic problem. In particular, when the initial and boundary conditions are piecewise constant, as shall be assumed in this work, the particular solution is also piecewise constant. Precisely, the x–t plane is divided into a number of regions by certain straight line segments (corresponding to the shocks), and in each region the state variables σ and v, and consequently T and ξ, are constant. Clearly, the field equations (2.2)–(2.4) are satisfied in the interior of each region. On the boundaries the solution must satisfy the jump equations (or initial/boundary conditions). It should be noted that the shocks result not only from the discontinuity of the initial/boundary conditions, but also from the non-smoothness of the constitutive functions at the start and the finish of phase transformations, as well as from the intersection of the characteristic curves.

In the remainder of this paper, we shall focus on the solutions of the jump equations.

4. Non-uniqueness of jump solutions. Maximum dissipation criterion

It is well known (e.g. Courant & Friedrichs 1956) that a nonlinear dynamic problem may admit weak solutions (jump solutions as termed here) even when the initial and boundary conditions are smooth. If weak solutions are allowed, uniqueness of solution is lost. As can be readily demonstrated, the jump equations (2.7)–(2.9) have infinitely many solutions that satisfy the given initial/boundary conditions.

Various criteria have been proposed (e.g. James 1980) to ensure the uniqueness. In this paper, we shall employ a criterion that is inspired by the entropy rate admissibility criterion proposed by Dafermos (1973). Roughly speaking, his criterion requires that for the admissible solution the total entropy decrease[2] with the highest possible rate. Similar criteria have been developed by Pence (1991, 1992).

[2] The entropy in Dafermos (1973) is defined mathematically, which corresponds to the negative of the physical entropy.

To adapt the idea to the present problem, we define internal dissipation of a material point by

$$\delta \equiv \rho T \eta_t - \pi \xi_t. \tag{4.1}$$

Following Truesdell (1969), the internal dissipation is interpreted as the amount by which the rate of change of entropy per unit coldness (reciprocal of temperature) exceeds the power of the thermodynamic force π conjugate to ξ. It follows from (2.19) that the internal dissipation δ is zero at a point where the solution is smooth, but is in general not zero at the shocks. The total internal dissipation is obtained by integrating δ over the rod

$$\Delta = \int_0^\infty (\rho T \eta_t - \pi \xi_t) \mathrm{d}x. \tag{4.2}$$

The integrand in (4.2) is taken in the sense of distribution as η and ξ may be discontinuous at a shock. In this work, we shall require that *the total internal dissipation of an admissible solution be maximum among all possible solutions.*

In virtue of (2.19), the total internal dissipation can be written as

$$\Delta = \sum s_t(-\rho \langle T \rangle [\![\eta]\!] + \langle \pi \rangle [\![\xi]\!]). \tag{4.3}$$

Here and henceforth, the summation is taken over all shocks. In deriving (4.3), use has been made of the equation

$$\lim_{\epsilon \to 0} \int_{s-\epsilon}^{s+\epsilon} f(x) g'(x) \mathrm{d}x = \langle f \rangle [\![g]\!].$$

By using (2.12), (2.14)–(2.17), (2.20) and (4.3), we can rewrite the total internal dissipation as

$$\Delta = \sum \rho s_t \left([\![G]\!] - [\![\sigma]\!] \left\langle \frac{\partial G}{\partial \sigma} \right\rangle - [\![T]\!] \left\langle \frac{\partial G}{\partial T} \right\rangle - [\![\xi]\!] \left\langle \frac{\partial G}{\partial \xi} \right\rangle \right). \tag{4.4}$$

The last expression possesses a certain mathematical structure which is a generalization of that in the analysis of Dafermos (1973). Let (σ^-, T^-, ξ^-) and (σ^+, T^+, ξ^+) be the left and right limits, respectively, of σ, T and ξ at a shock. The straight line segment joining these two points in the σ–T–ξ space can be represented in the following parametric form:

$$T(\sigma) = T^- + \frac{[\![T]\!]}{[\![\sigma]\!]}(\sigma - \sigma^-), \qquad \xi(\sigma) = \xi^- + \frac{[\![\xi]\!]}{[\![\sigma]\!]}(\sigma - \sigma^-). \tag{4.5}$$

Implied here is the notation $[\![T]\!] = T^+ - T^-$, etc. The value of the Gibbs free energy over this line segment is

$$\tilde{G}(\sigma) = G(\sigma, T(\sigma), \xi(\sigma)). \tag{4.6}$$

We define a generalized strain ε by

$$\varepsilon(\sigma) = -\rho \tilde{G}'(\sigma) = -\rho \left(\frac{\partial G}{\partial \sigma} + \frac{[\![T]\!]}{[\![\sigma]\!]} \frac{\partial G}{\partial T} + \frac{[\![\xi]\!]}{[\![\sigma]\!]} \frac{\partial G}{\partial \xi} \right). \tag{4.7}$$

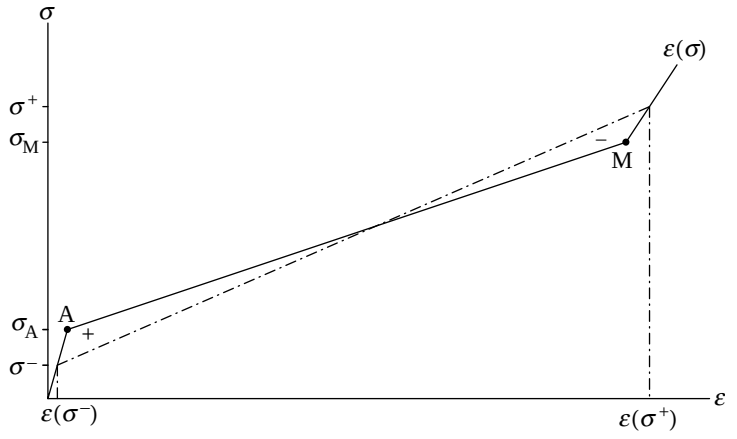

Figure 1. Graphical interpretation of the maximum dissipation criterion.

It then follows that

$$\frac{1}{2}(\sigma^+ - \sigma^-)[\varepsilon(\sigma^+) + \varepsilon(\sigma^-)] - \int_{\sigma^-}^{\sigma^+} \varepsilon(\sigma)\mathrm{d}\sigma$$
$$= \rho\left(\llbracket G\rrbracket - \llbracket\sigma\rrbracket\left\langle\frac{\partial G}{\partial\sigma}\right\rangle - \llbracket T\rrbracket\left\langle\frac{\partial G}{\partial T}\right\rangle - \llbracket\xi\rrbracket\left\langle\frac{\partial G}{\partial\xi}\right\rangle\right). \tag{4.8}$$

The right-hand side of (4.8) has appeared in (4.4), while the left-hand side is the (signed) area between the cord that joins $(\sigma^-, \varepsilon(\sigma^-))$ with $(\sigma^+, \varepsilon(\sigma^+))$ and the graph of $\varepsilon(\sigma)$, as depicted in figure 1 for a piecewise linear stress–strain diagram. We thus argue that the jump solution should be such that this area is maximum when $s_t > 0$, and is minimum when $s_t < 0$.

Hence, for a jump solution where shocks propagate from low stress region σ^- to high stress region σ^+ (i.e. $s_t > 0$), the solution with maximum total internal dissipation involves two shocks: one from σ^- to σ_M, and the other from σ_M to σ^+. The internal dissipation at the first shock is maximum while at the second shock is zero. On the other hand, for a jump solution where shocks propagate from σ^+ to σ^- ($s_t < 0$), the maximum internal dissipation criterion again renders two shocks: one from σ^+ to σ_A, and the other from σ_A to σ^-. For the SMA polycrystals studied in the present work, the stress–strain diagram is of the form of figure 1 with the segment A–M corresponding to the phase transformation between austenite and martensite.[3]

It must be pointed out that the above argument is presented primarily for the purpose of providing a suggestive guideline for selecting the admissible solutions in the numerical implementation to be presented in the sequel. The argument needs to be further developed in at least two aspects. Firstly, the effect of the propagation velocities s_t of shock waves on the internal dissipation

[3] For a typical Ni–Ti alloy, the forward and reverse transformations follow different paths. Figure 1 thus represents a part of the stress–strain diagram.

has not been accounted for. This effect is fully considered in Dafermos' (1973) work, where he shows, for two particular systems, that the effect of s_t does not alter the final solution, and that the maximum dissipation rate criterion is equivalent to the so-called viscosity criterion. Secondly, the generalized strain defined in (4.7) is not the physical strain which is used in the subsequent analysis, since it also involves the change of the Gibbs free energy due to the changes of temperature and martensitic volume fraction. Also, for the stress–strain curve derived in the sequel, the temperature and martensitic volume fraction do not change linearly in the stress, as is taken in (4.5). Nevertheless, a fairly extensive numerical investigation has indicated that the argument of maximizing (minimizing when $s_t<0$) the signed area does lead to the solution that has the maximum internal dissipation among all the solutions that have been tried. This area argument gives a simple and convenient way to visualize the maximum dissipation criterion. A rigorous analysis for this argument is the subject of further research.

5. An SMA constitutive function

We consider a specific form of the constitutive function for polycrystalline SMAs, which is developed by Lagoudas *et al.* (1996). The Gibbs free energy is of the form

$$G(\sigma, T, \xi) = -\frac{1}{2\rho}(S^{\mathrm{A}} + \xi\Delta S)\sigma^2 - \frac{\alpha}{\rho}\sigma(T - T_0) + c\left(T - T_0 - T\ln\frac{T}{T_0}\right) - (\eta_0^{\mathrm{A}} + \xi\Delta\eta_0)T + e_0^{\mathrm{A}} + \xi\Delta e_0 + \frac{1}{\rho}f(\xi), \tag{5.1}$$

$$\Delta S \equiv S^{\mathrm{M}} - S^{\mathrm{A}}, \qquad \Delta\eta_0 \equiv \eta_0^{\mathrm{M}} - \eta_0^{\mathrm{A}}, \qquad \Delta e_0 \equiv e_0^{\mathrm{M}} - e_0^{\mathrm{A}}, \tag{5.2}$$

where T_0 is the reference temperature, α the thermal expansion coefficient, c the specific heat, S^{A} and S^{M} the elastic compliances in the austenitic phase and martensitic phase, respectively, η_0^{A} and η_0^{M} the reference specific entropies, e_0^{A} and e_0^{M} the reference specific internal energies, and $f(\xi)$ the hardening function which physically represents the free energy of mixing. Here, it has been assumed that the thermal expansion coefficient and specific heat remain constant during the phase transformation.

A polynomial form of the hardening function is used, which reads

$$f(\xi) = \begin{cases} \dfrac{1}{2}\rho b^{\mathrm{M}}\xi^2 + \mu\xi + \dfrac{1-\xi}{1-\xi_{\mathrm{R}}}\left(f_{\mathrm{R}} - \dfrac{1}{2}\rho b^{\mathrm{M}}\xi_{\mathrm{R}}^2 - \mu\xi_{\mathrm{R}}\right) & \text{when } \xi_t > 0, \\ \dfrac{1}{2}\rho b^{\mathrm{A}}\xi^2 + \dfrac{\xi}{\xi_{\mathrm{R}}}\left(f_{\mathrm{R}} - \dfrac{1}{2}\rho b^{\mathrm{A}}\xi_{\mathrm{R}}^2\right) & \text{when } \xi_t < 0, \end{cases} \tag{5.3}$$

where μ, b^{A} and b^{M} are material constants, and ξ_{R} and f_{R} are the values of ξ and f, respectively, at which ξ_t previously changed sign. Substituting (5.1) and (5.3) into (2.17) and (2.18), we find that during phase transformations the value of ξ is

given by

$$\xi = \begin{cases} \dfrac{1}{\rho b^{\mathrm{M}}}\left(H|\sigma| + \dfrac{1}{2}\Delta S\sigma^2 + \rho\Delta\eta_0 T - \rho\Delta e_0 - Y + \dfrac{f_{\mathrm{R}} - \dfrac{1}{2}\rho b^{\mathrm{M}}\xi_{\mathrm{R}}^2 - \mu}{1-\xi_{\mathrm{R}}} \right) & \text{when } \xi_t > 0, \\ \dfrac{1}{\rho b^{\mathrm{A}}}\left(H|\sigma| + \dfrac{1}{2}\Delta S\sigma^2 + \rho\Delta\eta_0 T - \rho\Delta e_0 + Y - \dfrac{f_{\mathrm{R}} - \dfrac{1}{2}\rho b^{\mathrm{A}}\xi_{\mathrm{R}}^2}{\xi_{\mathrm{R}}} \right) & \text{when } \xi_t < 0. \end{cases} \tag{5.4}$$

The prescribed impact stress on the boundary is compressive. Hence, the stress and strain in the rod are non-positive. Substituting (5.1) into (2.12) and (2.14)–(2.16), we find that

$$\epsilon = S^{\mathrm{A}}\sigma + \alpha(T - T_0) + (\Delta S\sigma - H)\xi, \tag{5.5}$$

$$\eta = \frac{\alpha}{\rho}\sigma + c\ln\frac{T}{T_0} + \eta_0^{\mathrm{A}} + \Delta\eta_0\xi. \tag{5.6}$$

For numerical solutions, we choose the reference temperature to be $T_0 = 315$ K, and use the following values of the material constants for typical equiatomic NiTi SMA from Lagoudas *et al.* (1996):

$$\left.\begin{aligned} &S^{\mathrm{A}} = \frac{1}{70\times10^3\ \mathrm{MPa}},\quad S^{\mathrm{M}} = \frac{1}{30\times10^3\ \mathrm{MPa}},\quad \alpha = 10^{-5}\ \mathrm{K}^{-1},\quad H = 0.05, \\ &\rho = 6450\ \mathrm{kg\ m}^{-3},\quad \rho\Delta\eta_0 = -0.35\ \mathrm{MPa\ K}^{-1},\quad \rho b^{\mathrm{A}} = 7.0\ \mathrm{MPa},\quad \rho b^{\mathrm{M}} = 5.25\ \mathrm{MPa}, \\ &\mu + \rho\Delta e_0 = -106\ \mathrm{MPa},\quad Y = 3.76\ \mathrm{MPa},\quad \rho c = 2.12\ \mathrm{MPa\ K}^{-1}. \end{aligned}\right\} \tag{5.7}$$

Consider a complete loading–unloading cycle in which an SMA sample undergoes quasi-static loading from 0 to -700 MPa, followed by quasi-static unloading to 0 MPa. The corresponding stress–strain curve, obtained from first solving (2.19), (5.4) and (5.6) for T and ξ, and then substituting the result into (5.5), is shown in figure 2. During loading, the material remains austenitic phase until the compressive stress reaches about 165 MPa, at which the martensitic phase transformation starts. The transformation finishes at the stress level of 614 MPa. Further increase of stress level gives elastic loading in martensite. Upon unloading, the material first undergoes elastic unloading, and then starts reverse phase transformation at about 504 MPa, which finishes at about 17 MPa.

It is also observed that the stress–strain curve is approximately linear in austenite, in martensite, during the forward transformation, and during the reverse transformation. By the argument in §3, a dynamic solution is approximately piecewise constant when the boundary condition is piecewise constant. Such a solution is determined by jump equations (2.7), (2.8) and (2.20). We now turn our attention to such solutions.

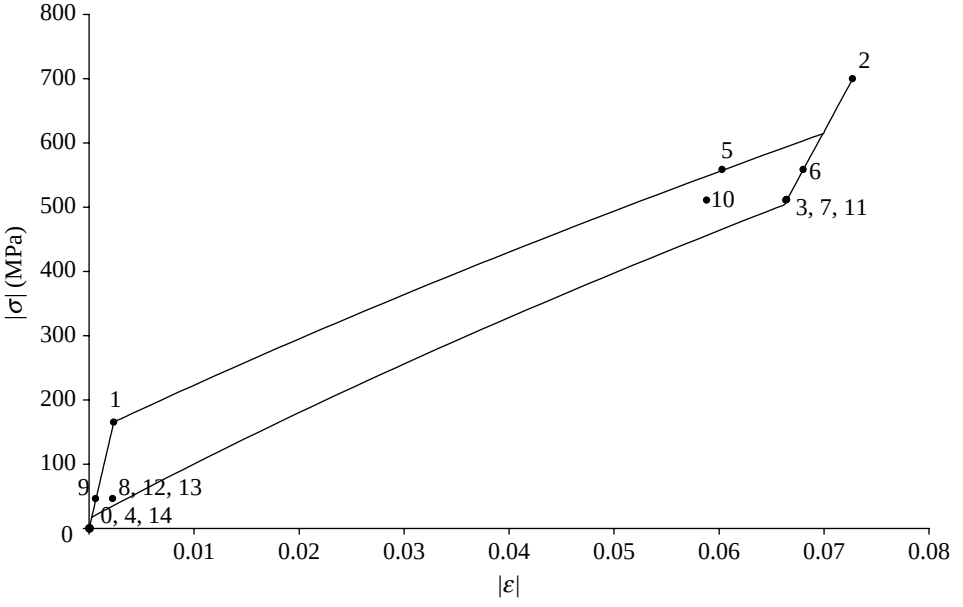

Figure 2. Stress–strain curve of the SMA under quasi-static loading/unloading.

6. Dynamic solution. Loading

We consider the dynamic solution for the SMA rod subjected to a rectangular impact load. The rod is initially at rest and in the austenitic phase, with zero stress and uniform temperature T_0. At the initial time, the end of the rod is subjected to an impact load of the duration $\tau = 5$ μs, and of the prescribed stress $\sigma_p = -700$ MPa, which exceeds the stress level at the finish of the martensitic transformation. The initial and boundary conditions are

$$v(x,0) = 0, \quad \sigma(x,0) = 0, \quad T(x,0) = T_0, \quad \xi(x,0) = 0, \qquad 0 \le x < \infty, \tag{6.1}$$

$$\sigma(0,t) = \begin{cases} \sigma_p & \text{when } 0 < t < \tau, \\ 0 & \text{when } \tau < t < \infty. \end{cases} \tag{6.2}$$

We shall search for piecewise constant solutions, in consideration of the piecewise constant boundary condition and the approximately piecewise linear stress–strain relation. A piecewise constant solution can be represented, in the x–t plane, by a number of polygonal regions, in each of which the state variables σ, ϵ, T and ξ are constant. The boundary of a polygonal region consists of either shock lines or the coordinate axis of the x–t plane. A solution procedure is to identify the shock lines and to determine the values of the state variables in each region, by using the jump equations, the transformation equations, and the maximum dissipation criterion.

At the initial stage of loading, there is a discontinuity of the stress at the origin $x=0$, $t=0$. This discontinuity will propagate into the rod in such a way that the jump equations (2.7), (2.8) and (2.20), as well as the transformation equation

(5.4) whenever applicable, are satisfied. There are, however, infinitely many solutions that meet the initial/boundary conditions near the origin. A unique solution is selected by the maximum dissipation criterion. A graphic interpretation of this criterion has been presented in §4. In the present situation, it amounts to finding a sequence of points on the stress–strain curve, such that the state variables corresponding to each consecutive pair of the points satisfy the jump equations and the transformation equations, and that the area between the sequence of the cords joining these points and the stress–strain curve is maximum. These requirements are met by three points, the first corresponding to the initial zero stress state, the second to the start of the martensitic transformation, and the third to the impact stress σ_{p}. The shock wave between the first and the second states is an elastic wave front, and that between the second and the third states is a matensitic phase transformation wave front.

Let these three states be denoted by indices 0, 1 and 2. The corresponding jump equations take the following form:

$$\left.\begin{aligned} a_{01}(\epsilon_0-\epsilon_1)+v_0-v_1=0, \quad \rho a_{01}(v_0-v_1)+\sigma_0-\sigma_1=0,\\ \rho(G_0+T_0\eta_0-G_1-T_1\eta_1)+\frac{1}{2}(\epsilon_0+\epsilon_1)(\sigma_0-\sigma_1)-H(-\sigma_0\xi_0+\sigma_1\xi_1)=0,\\ a_{12}(\epsilon_1-\epsilon_2)+v_1-v_2=0, \quad \rho a_{12}(v_1-v_2)+\sigma_1-\sigma_2=0,\\ \rho(G_1+T_1\eta_1-G_2-T_2\eta_2)+\frac{1}{2}(\epsilon_1+\epsilon_2)(\sigma_1-\sigma_2)-H(-\sigma_1\xi_1+\sigma_2\xi_2)=0, \end{aligned}\right\} \tag{6.3}$$

where a_{ij} is the propagation velocity s_t of the shock between the regions of states i and j, and G_i, ϵ_i and η_i are related to σ_i, T_i and ξ_i through (5.1), (5.3), (5.5) and (5.6). By the initial and boundary conditions, we have

$$v_0=0, \qquad \sigma_0=0, \qquad T_0=315, \qquad \xi_0=0, \qquad \sigma_2=-700.$$

Since State 2 is in martensite, we also have $\xi_2=1$. Furthermore, because State 1 is at the start of the martensitic transformation, it satisfies (5.4*a*) with $\xi_1=0$:

$$-H\sigma_1+\frac{1}{2}\Delta S\sigma_1^2+\rho\Delta\eta_0 T_1-\rho\Delta e_0-Y-\mu=0. \tag{6.4}$$

Here, it has been assumed that $\xi_{\mathrm{R}}=0$ and $f_{\mathrm{R}}=0$ initially.

The above algebraic equations are readily solved, yielding the numerical values of States 2 and 3, as well as the propagation velocities of the shocks, as follows:

$$\sigma_1=-165\ \mathrm{MPa}, \quad \epsilon_1=-0.236\%, \quad v_1=7.78\ \mathrm{m\,s^{-1}}, \quad T_1=315\ \mathrm{K}, \quad \xi_1=0,$$

$$\sigma_2=-700\ \mathrm{MPa}, \quad \epsilon_2=-7.27\%, \quad v_2=84.1\ \mathrm{m\,s^{-1}}, \quad T_2=375\ \mathrm{K}, \quad \xi_2=1,$$

$$a_{01}=3300\ \mathrm{m\,s^{-1}}, \quad a_{12}=1090\ \mathrm{m\,s^{-1}}.$$

We plotted these states in figure 2 as dots labelled by the corresponding number. It is found that these jump solutions lie very close to the quasi-static loading

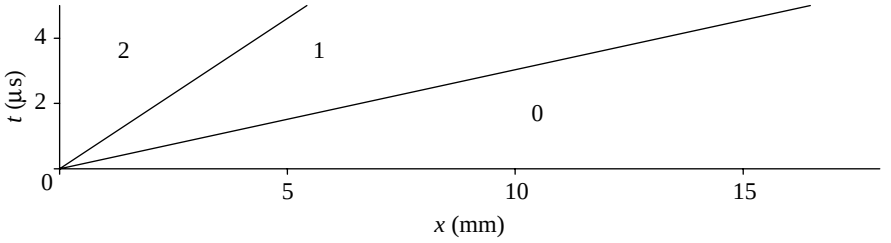

Figure 3. Shock waves and the regions of the piecewise constant solution during loading.

curve. It can be argued that the jump solutions and smooth solutions should coincide if the stress–strain relation is piecewise linear.

It is illustrative to also present the solutions graphically in the space–time plane (x–t plane). In figure 3, the two straight lines emanated from the origin represent the two shock waves discussed above, with the regions separated by them representing the states as labelled. The slopes of the straight lines are the slowness (reciprocal of the velocity) of the shock waves.

This solution is almost identical to that presented by Chen & Lagoudas (2000). In the previous work, a quadratic approximation is used for the term $T \ln T/T_0$ in the Gibbs free energy function (5.1). Also, the previous solution satisfies the maximum dissipation criterion exactly with the inclusion of a small region where the state variables are not constant but satisfy the field equations (2.2), (2.3) and (2.19). This region corresponds to a portion of the stress–strain curve near the start of martensitic transformation, followed by a jump to the full martensite at the impact stress. This gives a slightly higher internal dissipation than the present piecewise constant solution does. The reason for choosing the piecewise constant solution is to simplify the numerical analysis. The fully developed solution would be extremely complicated for unloading process to be considered in the present work. The difference between the present solution and the previous solution, however, is so small that it can be safely neglected in practice.

7. Dynamic solution. Unloading

As stated in §6, when $t=\tau=5$ μs, the stress at the impact end suffers a jump discontinuity from $\sigma_{\mathrm{p}}=-700$ MPa to zero, and remains zero thereafter. This discontinuity will again propagate into the rod in such a way that the jump equations (2.7), (2.8) and (2.20) are satisfied, and that the internal dissipation is maximum. For unloading, the task at hand is to find a sequence of points on the stress–strain curve, starting from State 2 and ending at zero stress, such that the area between stress–strain curve and the sequence of the cords joining these points is maximum. This requirement is met by two points, labelled as States 3 and 4. State 3 corresponds to the start of the reverse phase transformation, and State 4 to austenite at zero stress. The shock wave between States 2 and 3 is an elastic unloading wave front, and that between States 3 and 4 is a reverse phase transformation wave front.

The jump equations for States 2–4 are similar to (6.3). Since State 4 is in austenite, we have $\xi_4=0$. Moreover, State 3 is at the start of the reverse transformation with $\xi_3=1$. Hence, it must satisfy (5.4*b*)

$$1=\frac{1}{\rho b^{\mathrm{A}}}\left(-H\sigma_3+\frac{1}{2}\Delta S\sigma_3^2+\rho\Delta\eta_0 T_3-\rho\Delta e_0+Y-\frac{f_{\mathrm{R}}-\frac{1}{2}\rho b^{\mathrm{A}}\xi_{\mathrm{R}}^2}{\xi_{\mathrm{R}}}\right), \tag{7.1}$$

where ξ_{R} and f_{R} are the values of the martensitic volume fraction and the hardening function, respectively, when ξ_t previously changed sign in State 2. That is,

$$\xi_{\mathrm{R}}=1,\quad f_{\mathrm{R}}=\frac{1}{2}\rho b^{\mathrm{M}}+\mu. \tag{7.2}$$

The last expression was obtained by evaluating (5.3*a*) at $\xi=1$, $\xi_{\mathrm{R}}=0$ and $f_{\mathrm{R}}=0$.

These algebraic equations yield

$$\sigma_3=-512\ \mathrm{MPa},\quad \epsilon_3=-6.65\%,\quad v_3=70.6\ \mathrm{m\,s^{-1}},\quad T_3=375\ \mathrm{K},\quad \xi_3=1,$$

$$\sigma_4=0,\quad \epsilon_4=0.005\%,\quad v_4=-2.02\ \mathrm{m\,s^{-1}},\quad T_4=320\ \mathrm{K},\quad \xi_4=0,$$

$$a_{23}=2160\ \mathrm{m\,s^{-1}},\quad a_{34}=1090\ \mathrm{m\,s^{-1}}.$$

States 3 and 4 are also plotted in figure 2 as the labelled dots. It is observed that the stress level of State 3 is slightly higher than that of the start of the reverse transformation under quasi-static loading/unloading. In State 4, on the other hand, the stress is zero, while the strain is a very small number. The difference between States 0 and 4 is so small that they are indistinguishable graphically.

The two shock waves initiated at unloading and the corresponding regions of the piecewise constant solution, along with those occurred at loading as previously demonstrated, are plotted in figure 4. As mentioned earlier, the slopes of these shock lines represent the slowness (reciprocal of the velocity) of the shock waves. The velocity of a shock wave is proportional to the square root of the slope of the straight line connecting the two corresponding states on the stress–strain curve (figure 2). It is observed that the elastic loading wave has the highest velocity, followed by the elastic unloading wave. The velocities of the phase transformation waves are substantially lower. This reflects the fact that the austenite has a larger stiffness than the martensite does. The stiffness during the phase transformation is much smaller.

An interesting observation, which turns out to lead to great complexity of the solution, is that the elastic unloading wave, while being initiated after the two waves initiated at loading, has a higher velocity than that of the forward phase transformation wave and will eventually meet it. From that point on, the structure of the solution undergoes a drastic change, giving rise to much more complicated distributions of the state variables.

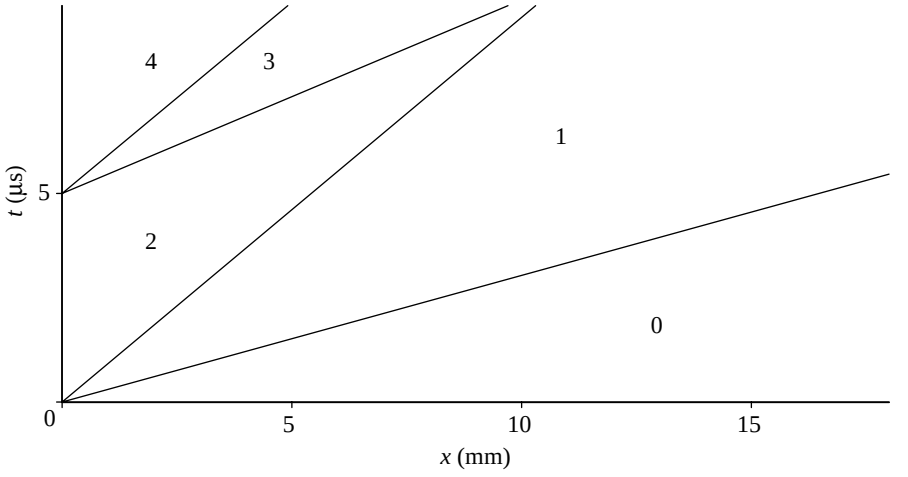

Figure 4. Shock waves and the regions of the piecewise constant solution during loading and initial stage of unloading.

8. Wave encounters

The encounter of the phase transformation wave initiated at loading and the elastic unloading wave occurs at point A with $x_A = 10.9$ mm, $t_A = 10.1$ μs. The subsequent solution in a neighbourhood of this point can be viewed as the solution for an initial value problem with t_A being the initial time. As the initial conditions, the values of state variables are given by those of State 3 on the left of x_A and by those of State 1 on the right of x_A. Physically, this amount to the collision of two pieces of the SMA rod that are initially in States 3 and 1, respectively. The two contact surfaces are required to remain in contact after the collision.

We again look for a piecewise constant solution that satisfies the jump equations, the transformation equations and the maximum dissipation criterion. Since the number of wave fronts and the material phase in each region of the solution are not known *a prior*, a selection procedure was implemented numerically to identify the desired solution.

The resulting solution has a structure similar to that of collision of two thermoelastic rods. Emanating from point A are three shock waves: a progressing wave with positive velocity, a reflecting wave with negative velocity, and a standing wave with zero velocity relative to the material point. Four regions of constant state variables are separated by these three shock waves. Two of them are the initial states: State 1 on the right of the progressing wave, and State 3 on the left of the reflecting wave. On the other sides of the progressing and reflecting waves are two new regions, labelled as State 5 and State 6, respectively. These two states, separated by the standing wave, have the same stress and the same velocity, as required by equations (2.7) and (2.8), but different temperatures, martensitic volume

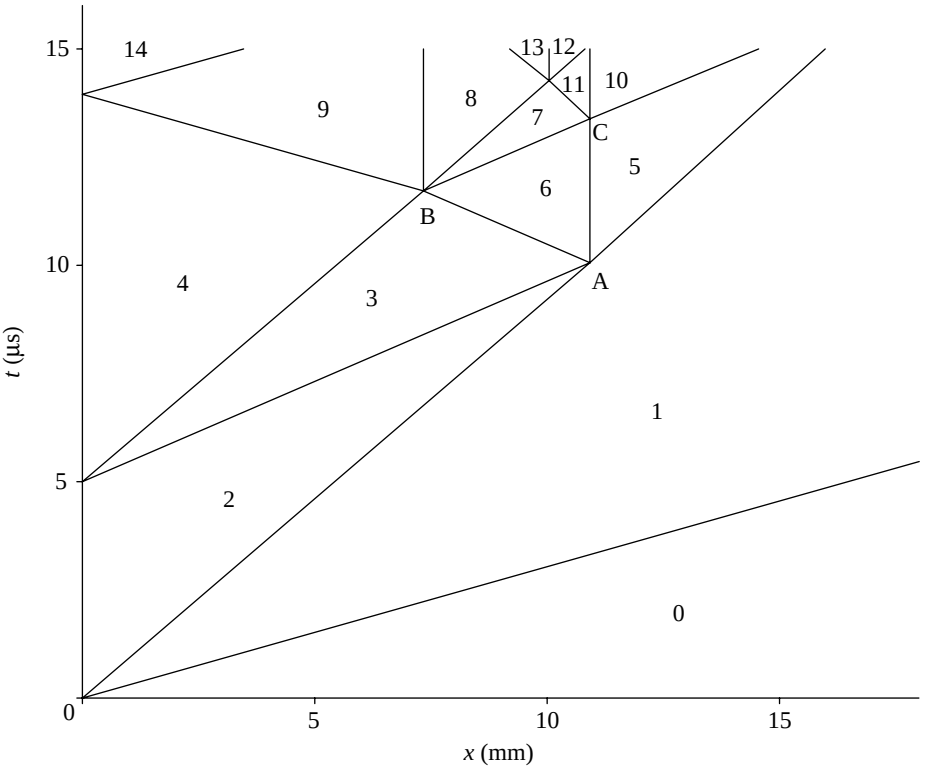

Figure 5. Shock waves and various regions of the piecewise constant solution.

fractions and strains. The numerical values of these two states are as follows:

$$\sigma_5 = -559\ \text{MPa}, \quad \epsilon_5 = -6.03\%, \quad v_5 = 67.2\ \text{m s}^{-1}, \quad T_5 = 366\ \text{K}, \quad \xi_5 = 0.871,$$

$$\sigma_6 = -559\ \text{MPa}, \quad \epsilon_6 = -6.80\%, \quad v_6 = 67.2\ \text{m s}^{-1}, \quad T_6 = 375\ \text{K}, \quad \xi_6 = 1,$$

$$a_{15} = 1030\ \text{m s}^{-1}, \quad a_{56} = 0, \quad a_{36} = -2160\ \text{m s}^{-1}.$$

These solutions are plotted in figures 2 and 5. It is observed that a material point on the right of point A undergoes a partial martensitic transformation as the progressing wave passes. On the other hand, a material on the left of point A is loaded elastically as the reflecting wave passes. A remark here is that it is not peculiar that the both points attain a higher stress level as the result of the collision. Indeed, since the velocity of State 3 is much larger than that of State 1, a strong compressive impact is created at collision, resulting in the both pieces being further compressively loaded.

The next wave encounter occurs at point B with $x_B = 7.34$ mm, $t_B = 11.7$ μs when the reflecting wave meets the reverse transformation wave initiated at unloading. This amounts to State 6, with high energy in martensite, colliding with State 4 which is stress free in austenite. The solution was found by the same method discussed above. It is found that this wave

encounter results in four shock waves: two progressing waves, one reflecting wave and one standing wave. The presence of two progressing waves is to satisfy the maximum dissipation criterion. A material point in the region of State 6 is first unloaded elastically, as the first progressing wave passes, to State 7 corresponding to the start of reverse phase transformation, and is further unloaded, at the passing of the second progressing wave, to State 8 which is near the finish of reverse phase transformation. A material point in the region of State 4, on the other hand, is elastically loaded to State 9 as the reflecting wave passes. Again, States 8 and 9 have the same stress and velocity, but different temperatures, martensitic volume fractions, and strains. States 7–9 are again plotted in figures 2 and 5, with numerical values as shown below:

$$\sigma_7 = -512\ \text{MPa}, \quad \epsilon_7 = -6.65\%, \quad v_7 = 63.8\ \text{m s}^{-1}, \quad T_7 = 375\ \text{K}, \quad \xi_7 = 1,$$

$$\sigma_8 = -46.5\ \text{MPa}, \ \epsilon_8 = -0.226\%, \ v_8 = -4.21\ \text{m s}^{-1}, \ T_8 = 321\ \text{K}, \ \xi_8 = 0.0325,$$

$$\sigma_9 = -46.5\ \text{MPa}, \quad \epsilon_9 = -0.062\%, \quad v_9 = -4.21\ \text{m s}^{-1}, \quad T_9 = 320\ \text{K}, \quad \xi_9 = 0,$$

$$a_{67} = 2160\ \text{m s}^{-1}, \quad a_{78} = 1060\ \text{m s}^{-1}, \quad a_{89} = 0, \quad a_{49} = -3300\ \text{m s}^{-1}.$$

Another interesting feature is revealed by the solution at the next encounter at point C with $x_C = 10.9$ mm, $t_C = 13.4$ μs (see figure 5). A material point in the region of State 7 undergoes a slightest partial reverse phase transformation to State 11, of which the values of the state variables are almost same as those of State 7. At the same time, a material point in the region of State 5 is elastically unloaded to State 10. Since State 5 is in a partial martensite, the elastic unloading takes place within the loop of the stress–strain diagram of complete phase transformations, as shown in figure 2.

The subsequent solution can be found in a similar manner. As time progresses, more wave encounters occur, resulting in more shock waves, more regions of constant state variables, and consequently even more wave encounters. The frequency and density of the wave encounters increase rapidly.

The stress, strain and temperature profiles at a few time instants $t = 5$, 10 and 15 μs are plotted in figures 6–8. There are clear correspondences between these figures and the shock wave diagram figure 5, as well as the stress–strain curve figure 2. Indeed, the locations of the jumps appearing in figures 6–8 can be observed in figure 5 as the intersections of the horizontal line of the particular time instant and the shock waves. It is noted that figures 6–8 have different length scales from that of figure 5, in order to display the entirety of the first elastic wave at $t = 15$ μs. The amount of stress jumps and strain jumps in figures 6 and 7 can also be observed in figure 2 as the differences of the two labelled states on the two sides of the shock.

Figures 6–8 show that a section with large stress, large strain and high temperature is initiated upon impact and propagates into the rod with decreasing magnitude as time progresses. Such a decrease is the result of the wave encounters described above. It is also observed that there is a temperature

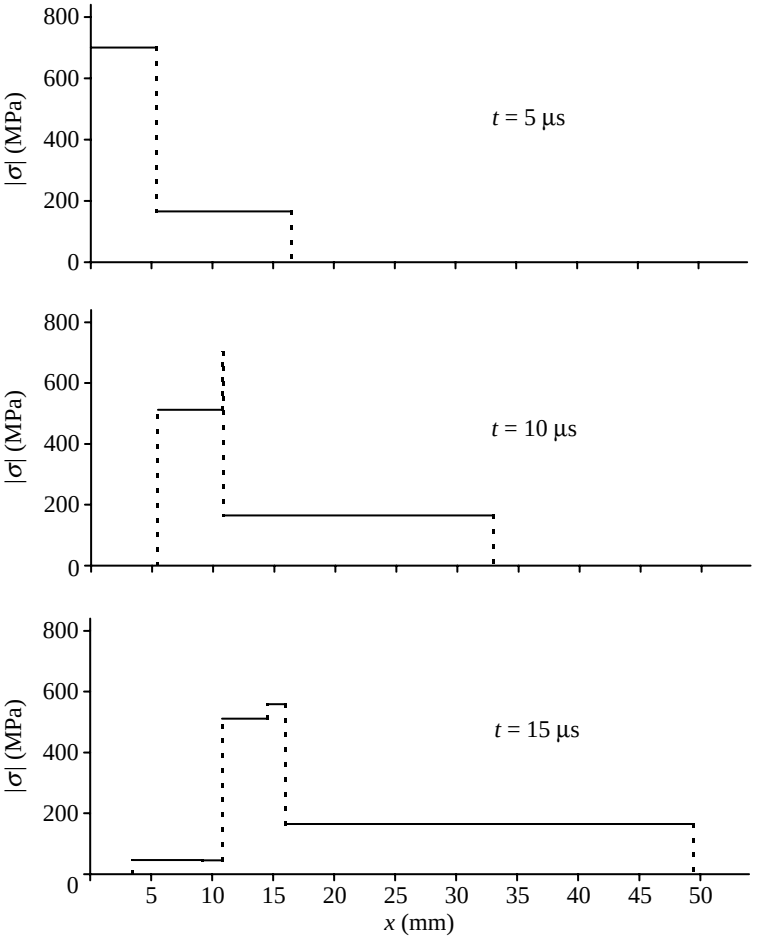

Figure 6. Stress profiles at various times.

difference as large as 60 K, along with large stress and strain differences, between the austenitic and martensitic phases.

Although an analytical solution for large values of t is not available, the following asymptotic behaviour of the solution is suggested by numerical simulations. Because of the zero stress on the end of the rod after impact, the stresses in the regions developed from regions 8–14 in figure 5 through sequential wave encounters all tend to zero as t approaches infinity. On the other hand, region 1, having the highest possible propagation speed, remains intact and will propagate indefinitely into the rod. Its right boundary, the elastic loading wave front, will propagate at the elastic acoustic speed $a_{01}=3300\ \mathrm{m\ s^{-1}}$ as shown in figure 5. Its left boundary, evolved from sequential wave encounters, will eventually approach the same propagation speed. Hence, after a certain amount of time, an elastically deformed band of an estimated length of 0.1 m emerges and propagates, at speed a_{01}, in the rod. The main body of the elastic band, which is fairly well defined after $t=50\ \mu\mathrm{s}$, is in region 1 with stress $\sigma=-165\ \mathrm{MPa}$. The stress is zero ahead of the elastic band and is essentially zero behind the band.

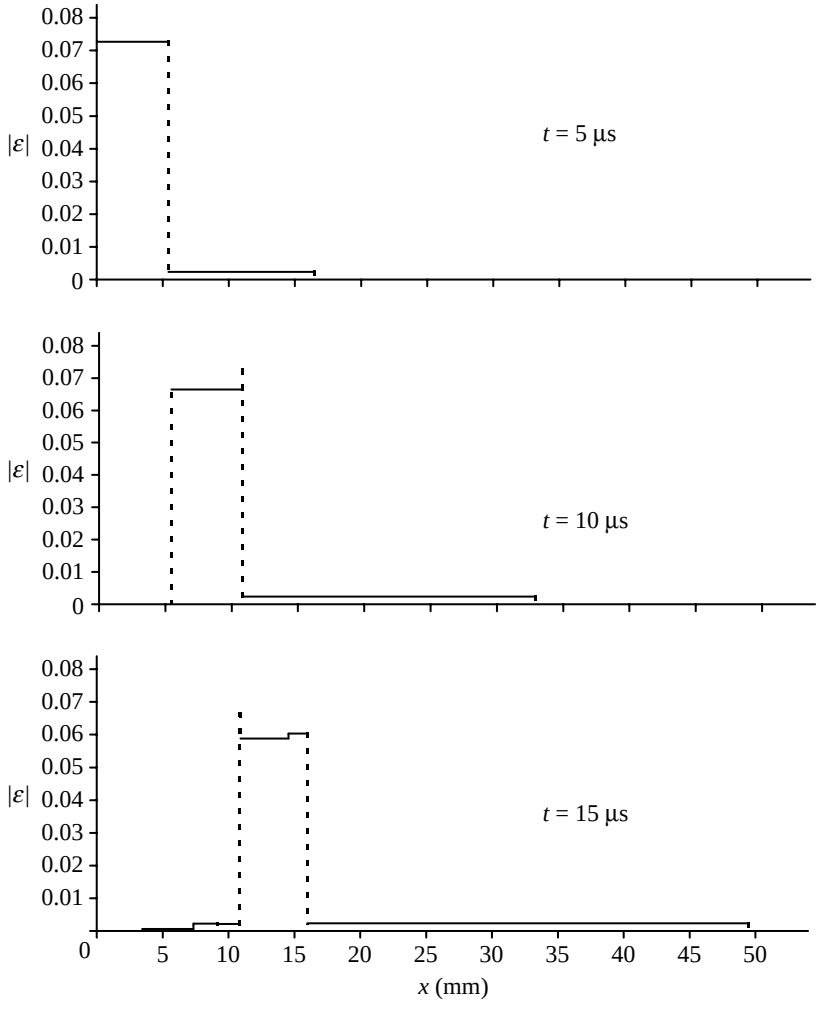

Figure 7. Strain profiles at various times.

A detailed analysis of this asymptotic behaviour of the solution will be presented elsewhere.

Mechanical energy may dissipate at a shock wave, either in the form of thermal dissipation or phase transformation dissipation. Detailed discussions of the various mechanisms of energy dissipation can be found in Pence (1992). For the present problem, the total energy dissipation can be calculated from the difference between input impact energy and the remaining elastic energy in the elastic band. It has been found that more than 90% of the impact energy is dissipated when the elastic band mentioned above is formed at $t=50$ μs. This indicates possible applications of the SMAs as materials for energy absorption devices under impact loads.

As a concluding remark, it is noted that the relatively high initial temperature ($T_0=315$ K) has been chosen in this work to have the martensitic transformation and complete reverse transformation in the initial loading/unloading stage. For

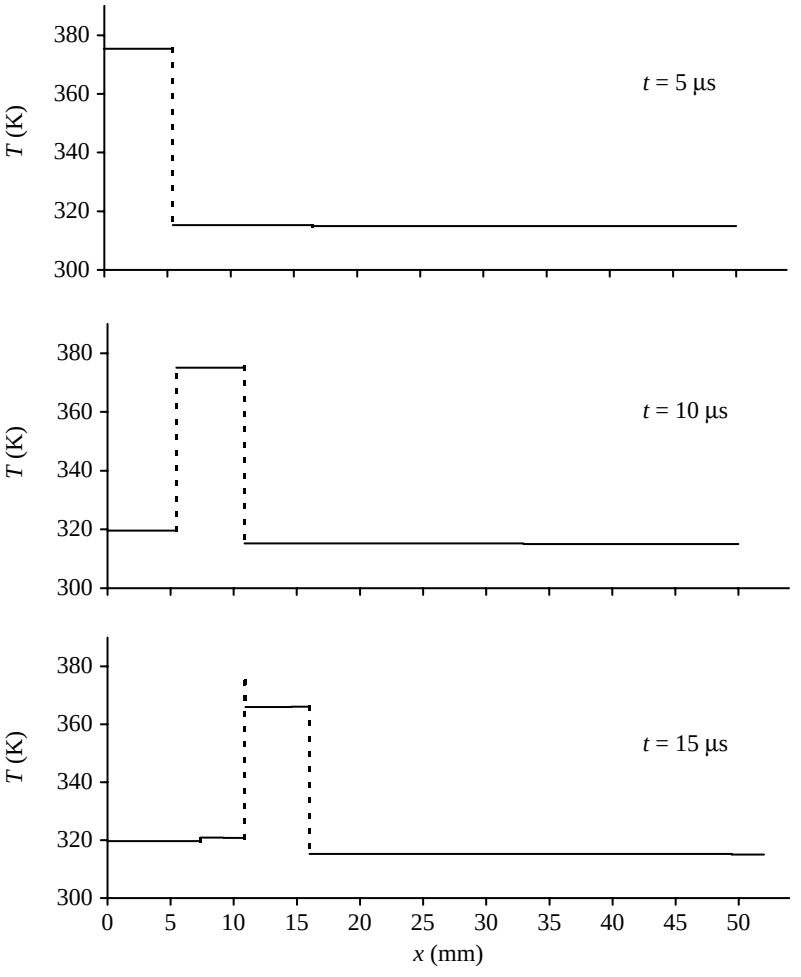

Figure 8. Temperature profiles at various times.

a lower initial temperature, the material may have only partial reverse transformation upon loading, or may initially be in twinned martensite and undergo detwinning at loading. In these cases, the dynamic solution under impact loads will be different from that discussed in this work, but may still be of interest. The present case, with the largest hysteresis loop, offers the highest degree of energy dissipation under impact loads.

The authors wish to acknowledge the supports of ONR grant no. M00014-99-1-1069 and the Texas Institute for Intelligent Bio-Nano Materials and Structures for Aerospace Vehicles, funded by NASA Cooperative Agreement No. NCC-1-02038. Y.-C.C. wishes to acknowledge the support of ARO grant 46828-MS-ISP.

References

Abeyaratne, R. & Knowles, J. K. 1991 Kinetic relations and the propagation of phase boundaries in solids. *Arch. Rational Mech. Anal.* **114**, 119–154. (doi:10.1007/BF00375400.)

Abeyaratne, R. & Knowles, J. K. 1994*a* Dynamics of propagating phase boundaries: thermoelastic solids with heat conduction. *Arch. Rational Mech. Anal.* **126**, 203–230. (doi:10.1007/BF00375642.)

Abeyaratne, R. & Knowles, J. K. 1994*b* Dynamics of propagating phase boundaries: adiabatic theory for thermoelastic solids. *Physica D* **79**, 269–288.

Bekker, A., Jimenez-Victory, J. C., Popov, P. & Lagoudas, D. C. 2002 Impact induced propagation of phase transformation in a shape memory alloy rod. *Int. J. Plast.* **18**, 1447–1479. (doi:10.1016/S0749-6419(02)00025-6.)

Bland, D. R. 1969 *Nonlinear dynamic elasticity*. New York: Blaisdell.

Chen, Y. C. & Lagoudas, D. C. 2000 Impact induced phase transformation in shape memory alloys. *J. Mech. Phys. Solids* **48**, 275–300. (doi:10.1016/S0022-5096(99)00044-7.)

Courant, R. & Friedrichs, K. O. 1956 *Supersonic flow and shock waves*. New York: Interscience.

Dafermos, C. M. 1973 The entropy rate admissibility criterion for solutions of hyperbolic conservative laws. *J. Differ. Equations* **14**, 202–212. (doi:10.1016/0022-0396(73)90043-0.)

James, R. D. 1980 The propagation of phase boundaries in elastic bars. *Arch. Rational Mech. Anal.* **73**, 125–158. (doi:10.1007/BF00258234.)

Lagoudas, D. C., Bo, Z. & Qidwai, M. A. 1996 A unified thermodynamic constitutive model for SMA and finite element analysis of active metal matrix composites. *Mech. Compos. Mater. Struct.* **3**, 153–179. (doi:10.1002/(SICI)1234-986X(199606)3:2<153::AID-MCM36>3.3.CO;2-J.)

Lagoudas, D. C., Ravi-Chandar, K., Sarh, K. & Popov, P. 2003 Dynamic loading of polycrystalline shape memory alloy rods. *Mech. Mater.* **35**, 689–716. (doi:10.1016/S0167-6636(02)00199-0.)

Lax, P. D. 1973 Hyperbolic systems of conservation laws and the mathematical theory of shock waves. In *Conf. Board Math. Sci. Regional Conf. Ser. Appl. Math.*, vol. 11. Philadelphia, PA: Society for Industrial and Applied Mathematics.

Pence, T. J. 1986 On the emergence and propagation of a phase boundary in an elastic bar with a suddenly applied end load. *J. Elast.* **16**, 3–42. (doi:10.1007/BF00041064.)

Pence, T. J. 1991 On the encounter of an acoustic shear pulse with a phase boundary in an elastic material: energy and dissipation. *J. Elast.* **26**, 95–146.

Pence, T. J. 1992 On the mechanical dissipation of solutions to the Riemann problem for impact involving a two-phase elastic material. *Arch. Rational Mech. Anal.* **117**, 1–52. (doi:10.1007/BF00375158.)

Truesdell, C. 1969 Rational thermodynamics, p. 30. New York: McGraw-Hill.

As this paper exceeds the maximum length normally permitted, the authors have agreed to contribute to production costs.